INORGANIC MATERIALS
AND NANOMATERIALS

Investigation of the Physicochemical Properties of Ceramics in the $Sm_2O_3-Y_2O_3-HfO_2$ System for Developing Promising Thermal Barrier Coatings

E. N. Kablov[a], O. N. Doronin[a], *, N. I. Artemenko[a],
P. A. Stekhov[a], P. S. Marakhovskii[a], and V. L. Stolyarova[b]

[a]*All-Russian Research Institute of Aviation Materials, Moscow, 105005 Russia*
[b]*St. Petersburg State University, St. Petersburg, 199034 Russia*
*e-mail: o-doronin@mail.ru

Abstract—The effect of components of ceramics in the $Sm_2O_3-Y_2O_3-HfO_2$ system on their thermophysical properties was studied. It was shown that the most stable materials at 1400°C are ternary ceramics in the system under investigation that contain ≤12.5 mol % Sm_2O_3; the thermal conductivity of these materials does not exceed 1.3 W/(m K). Increasing samarium oxide content in samples in the $Sm_2O_3-Y_2O_3-HfO_2$ system was found to lead to significant changes in phase equilibria at temperatures ≥1000°C. The effect of the contents of individual components of the studied ceramics on the thermal conductivity and the linear thermal expansion coefficient, which largely determine the suitability of a ceramic material for using in a thermal barrier coating. It was shown that the addition to 12.5 mol % samarium oxide ensures the stability of the linear thermal expansion coefficient at acceptable values of the thermal conductivity of 0.8–1.6 W/(m K).

INTRODUCTION

Thermal barrier coatings (TBC) are the most widely used means of increasing the hot-end component life in modern gas turbine engines [1–4]. The protective effect of such coatings is ensured by the fact that the ceramic layer in TBC at operating temperatures has a thermal conductivity of about 2–4 W/(m K), which is significantly lower than the thermal conductivity of the material (substrate) to which the coating is applied. In the vast majority of cases, the substrate materials are heat-resistant nickel alloys with a thermal conductivity of $\lambda \geq 18-20$ W/(m K) [5, 6]. In practice, if there is intense heat removal from the substrate material over a thickness of the TBC ceramic layer of 70–200 μm, then there is a temperature difference to 50–150°C, depending on the thermal conductivity of the ceramic layer.

Currently, the most popular materials for producing TBC ceramic layers are ceramics in the $ZrO_2-(7-8\%)Y_2O_3$ system [7–9]. This is due to a unique combination of the physicomechanical and thermophysical characteristics: at a thermal conductivity of $\lambda = 1.95-2.44$ W/(m K) [10], the linear thermal expansion coefficient (LTEC) is $(8-10) \times 10^{-6}$ 1/K [11]. The structural and phase stability of such ceramic systems is preserved until 1200–1250°C, after which the ceram-

ics begins to crack because of phase transitions, sintering, and volume changes.

Modern gas turbine engines are designed under new requirements for increasing the operating temperatures of the hot-end component surface to 1300–1350°C [12, 13]. This necessitates the search for new ceramic materials or the use of multilayer ceramic coatings in which a layer with higher high-temperature stability is produced on the surface of conventional ceramic materials in the $ZrO_2-(7-8\%)Y_2O_3$ system. Although a wide diversity of experimental studies on this subject were made [7, 8, 11–14], they failed to find ceramic materials that would ensure that the operating temperatures of the surface of hot-end components of commercial gas turbine engines are ≥1300°C. In this context, of particular importance are investigations of the physicochemical properties of ceramics in multicomponent systems containing oxides of zirconium, hafnium, yttrium, samarium, holmium, lanthanum, and other rare and rare-earth metals [15, 16].

In developing and studying new-generation ceramics for thermal barrier coatings, it is most important to either ensure the structural stability of the material, or decrease its thermal conductivity. One of the examples of such an approach is to produce TBC thermal barrier layers from rare-earth metal zirconates with the gen-

eral quasi-stoichiometric formula $Ree_2Zr_2O_7$, where Ree are rare-earth metals of the yttrium (Y, La, Gd–Lu) and cerium (Ce–Eu) subgroups. The best-studied rare-earth metal zirconate is gadolinium zirconate $Gd_2Zr_2O_7$, which has a thermal conductivity in the sintered state of ~1.0 W/(m K) [16–18]. However, using it as a single ceramic layer in TBC meets with difficulties because of low LTEC ($\lambda = (6–8) \times 10^{-6}$ 1/K) [18–20], which necessitates the use of an intermediate ceramic layer made of conventional ceramic materials in the $ZrO_2–(7–8\%)Y_2O_3$ system. Because there is a great variety of designs and compositions of TBC ceramic layers serviceable at temperatures >1300°C, it is most expedient to determine the main properties of ceramics that make it possible to use the ceramics in TBC (first of all, LTEC and thermal conductivity) and then study the structural and phase stability of the ceramics with the most optimal compositions.

Note that the use of ternary and more-component ceramics for applying TBC ceramic layers is quite wide and is well ahead of fundamental studies in this field. For example, Oerlikon Metco AG manufactures commercial powders Metco 205NS and Metco 206A for thermal spraying of the systems Zr–Ce–Y–O and Zr–Y–Gd–Yb–O, respectively [21].

This work is one of the first in the series of investigations of the effect of the composition of oxide ceramics on the physicochemical properties that determine the advisability of using the ceramics in TBC.

The most promising alternative to conventional materials in the $ZrO_2–(7–8\%)Y_2O_3$ system are ceramics based on hafnium oxide. The most important advantages of hafnium oxide are its high-temperature stability and the absence of phase transitions in the temperature range to 1700°C, a high melting point (2900°C), and a low thermal conductivity at temperatures above 1000°C ($\lambda \leq 1.8–2.9$ W/(m K)) [7, 8]. The main disadvantage of hafnium oxide for using as a ceramic layer in a thermal barrier coating is a low LTEC $(6.1–7.06) \times 10^{-6}$ 1/K. Previous studies of ceramics based on hafnium oxide, stabilized by yttrium oxide, with LTEC $> 8.0 \times 10^{-6}$ 1/R at temperatures >1000°C showed that ceramics based on hafnium oxide can be promising for using in TBC for heat-resistant nickel alloys [15]. It should be taken into account that, in the $Y_2O_3–HfO_2$ at Y_2O_3 contents <90%, polymorphic transformations begin at temperatures as low as ~900°C [22, 23]; this can cause unacceptable variations of LTEC and reduce the thermal cycling stability of the coatings.

The investigation of the phase diagram of the system $Sm_2O_3–Y_2O_3–HfO_2$ [24, 25] showed that structures of the pyrochlore $Sm_2Hf_2O_7$ type can form in it. However, the published data on the physicochemical properties of the system $Sm_2O_3–Y_2O_3–HfO_2$ are few and insufficient for making an unambiguous choice and substantiating the advisability of using the most

promising samples of this system in TBC. Available in the literature, the state diagrams of both the ternary system $Sm_2O_3–Y_2O_3–HfO_2$ [24, 25], and the binary systems $Sm_2O_3–Y_2O_3$ [24, 25], $Sm_2O_3–HfO_2$ [26], and $Y_2O_3–HfO_2$ [22, 23] can be extremely useful in analyzing the results of studying the physicochemical properties of the ceramics samples tested in this work.

EXPERIMENTAL

The initial materials for the synthesis of samples of ceramics in the system $Sm_2O_3–Y_2O_3–HfO_2$ were powder mixtures of the corresponding oxides, the content of the main component in which was the following: Sm_2O_3, 99.98 wt %; Y_2O_3, 99.999 wt %; and HfO_2, 99.9 wt %.

For the solid-phase synthesis of samples, a batch (20–30% of weight) of the initial powder of each of the oxides was sampled and ground to a fraction 5 μm, and the remaining coarse fraction was screened out. The materials for the solid-state synthesis were mixed in the ratio of 80% of the fraction 5–100 μm and 20% of the fraction 0–5 μm. The mixtures for the solid-phase synthesis were prepared according to the compositions indicated in the Synth. rows in Table 1. The components of the mixtures were weighed on a Sartorius BP 221S analytical balance (Germany) with an accuracy to 0.0001 g. After obtaining the process mixture, to 5% polyvinyl alcohol was added to it. Figure 1 presents the state diagram of the system $Sm_2O_3–Y_2O_3–HfO_2$, in which the synthesized experimental compositions are indicated [26, 27].

The obtained reaction mixture was compacted into cylindrical samples 30 ± 5 mm high and 32 ± 3 mm in diameter. Then the samples were subjected to multistage heat treatment: low-temperature heat treatment at 350°C for 2 h for the uniform removal of the organic bond, and then high-temperature heat treatment at a temperature above 1600°C for 6 h for the solid-phase synthesis and the reduction of the open porosity. The presence of the fraction ≤5 μm in the process mixture ensured the sintering of the samples of all the experimental compositions, and the presence of coarse particles to 100 μm in size made it possible to study the mechanisms of the formation of ceramic materials in the solid-phase synthesis.

The experimental compositions after the solid-phase synthesis were identified by metallographic and metallophysical studies with a Quanta Inspect F50 scanning electron microscope (FEI, The Netherlands) using an EDAX energy-dispersive spectroscopy system (USA). The integral average (over the region 1000 × 1000 μm) contents of the main elements (Sm, Y, and Hf) in the samples were determined to confirm the agreement between the compositions of the synthesized samples to the calculated compositions (as synthesized). The contents of the main elements in the synthesized samples are presented in the Anal. rows of

Table 1. Experimental compositions of ceramic materials in the system Sm_2O_3–Y_2O_3–HfO_2

No. of composition	Composition*	Oxide content, mol %			Metal content, wt %		
		Sm_2O_3	Y_2O_3	HfO_2	Sm	Y	Hf
1	Synth.	70.0	30.0	0	79.78	20.22	0
	Anal.				78.10 ± 4.45	21.90 ± 1.26	0
2	Synth.	50.0	50.0	0	62.84	37.16	0
	Anal.				61.13 ± 3.05	38.87 ± 2.86	0
3	Synth.	50.0	0	50.0	62.75	0.00	37.25
	Anal.				60.60 ± 3.63	0.00	39.40 ± 1.64
4	Synth.	37.5	31.25	31.25	50.32	24.79	24.89
	Anal.				50.60 ± 2.49	25.42 ± 1.97	23.98 ± 1.80
5	Synth.	25	37.5	37.5	36.01	31.93	32.06
	Anal.				37.17 ± 2.52	30.39 ± 2.20	32.44 ± 2.08
6	Synth.	12.5	43.75	43.75	19.43	40.21	40.36
	Anal.				19.78 ± 1.57	39.35 ± 1.63	40.87 ± 2.24
7	Synth.	50.0	12.5	37.5	62.77	9.28	27.95
	Anal.				64.44 ± 4.17	9.60 ± 0.65	25.96 ± 1.04
8	Synth.	37.5	15.62	46.88	50.29	12.39	37.32
	Anal.				52.41 ± 2.76	12.19 ± 0.70	35.40 ± 1.93
9	Synth.	25	18.75	56.25	35.98	15.96	48.06
	Anal.				37.47 ± 2.88	16.36 ± 0.87	46.17 ± 3.42
10	Synth.	12.5	21.82	65.68	19.41	20.04	60.55
	Anal.				20.18 ± 1.09	20.41 ± 1.32	59.41 ± 4.56
11	Synth.	0	10.0	90	0.00	9.97	90.03
	Anal.				0.00	9.55 ± 0.40	90.45 ± 6.94
12	Synth.	10.0	0	90	15.77	0.00	84.23
	Anal.				16.32 ± 0.99	0.00	83.68 ± 4.02
13	Synth.	10.0	10.0	80.0	15.77	9.33	74.90
	Anal.				16.44 ± 1.12	9.56 ± 0.63	74.00 ± 4.11

* The Synth. rows represent the compositions of the initial mixture for the solid-phase synthesis; the Anal. rows, the integral average contents (weight percentages) of the main component in the synthesized material.

Table 1. The average discrepancy between the calculated compositions and the compositions of the synthesized samples does not exceed 14%; the relatively high discrepancy in the composition is explained by the error of electron microprobe analysis. The results of a more detailed investigation of the chemical and phase composition of samples in the system Sm_2O_3–Y_2O_3–HfO_2 by the solid-phase synthesis method are presented in our most recent work [28].

The thermophysical properties of the experimental samples were studied in the temperature range 20–1400°C according to standard procedures. The specific heats of the samples were determined by differential scanning calorimetry with a Netzsch DSC 404 F1 calorimeter (Germany); the thermal diffusivity, by the laser flash method with a Netzsch LFA 427 laser flash apparatus; the density, by hydrostatic weighing with an A&D GR 200 analytical balance (Japan); and LTEC, by dilatometry with a Netzsch DIL402C dilatometer.

To study the physicochemical properties, three samples of each of the compositions were synthesized; if there were significant (>15%) deviations in values of the physicochemical properties, an additional synthesis of a sample of the same composition was performed. In further calculations, the data on three samples closest in physicochemical properties were taken into account.
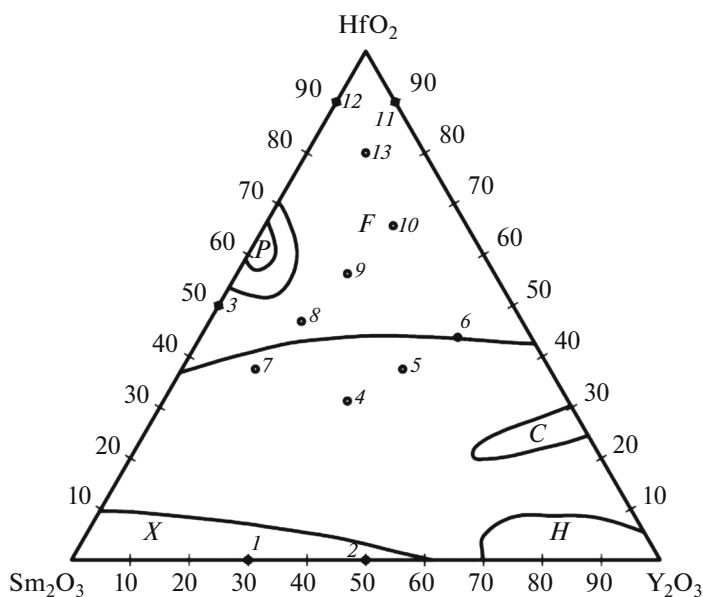
Fig. 1. State diagram of the system $Sm_2O_3-Y_2O_3-HfO_2$ [22−24].

The thermal conductivity $\lambda(T)$ of a sample of a studied composition was calculated from the obtained data by the formula [30]

$$\lambda(T) = \alpha(T)\rho(T)C_p(T), \qquad (1)$$

where $\alpha(T)$ is the thermal diffusivity, m^2/s; $\rho(T)$ is the density, kg/m^3; and $C_p(T)$ is the specific heat, J/(kg K).

LTEC was measured in 13 samples of ceramics in the system $Sm_2O_3-Y_2O_3-HfO_2$, the compositions of which are presented in Table 1, in the temperature range 200−1400°C. Figure 2 illustrates the measurement results.

The measurement results showed that LTEC in samples 2, 4, 8, 9, 11, and 12 abruptly decreases at temperatures >1000°C. In samples 1, 3, 5−7, 10, and 12, LTEC monotonically changes within a given range.

The specific heat was measured in 13 samples of ceramics in the system $Sm_2O_3-Y_2O_3-HfO_2$, the compositions of which are given in Table 1, in the temperature range 20−1400°C. Figure 3 presents the measurement results. The specific heats of all the 13 samples are seen to monotonically increase. The specific heat is lowest in samples 3 and 11−13; meanwhile, the hafnium content in samples 11−13 was 80−90 mol %, or 74.5−89.3 wt %.

The density was measured in 13 samples of ceramics in the system $Sm_2O_3-Y_2O_3-HfO_2$, the compositions of which are given in Table 1, and using LTEC, the densities in the temperature range 20−1400°C were found. Figure 4 shows the measurement results. The measurements demonstrated that the densities of samples 1−13 at room temperature are within the range 3970−6810 kg/m^3.

Taking into account the densities of individual oxides of samarium, yttrium, and hafnium, which are 8350, 5010, and 9680 kg/m^3, respectively [10], one can be concluded that the sintered cylindrical samples have a porosity of about 20−25%, which corresponds to the porosity of TBC ceramic layers produced by atmospheric plasma deposition [7]. Note that the anomalous increase in the density of ceramics of compositions 2, 4, 8, 11, and 12 at temperature above 1300°C is fully consistent with the decrease in LTEC.

The thermal diffusivity was measured in 13 samples of ceramics in the system $Sm_2O_3-Y_2O_3-HfO_2$, the compositions of which are given in Table 1, in the temperature range 20−1400°C. Figure 5 presents the measurement results.

The measurements showed that the thermal diffusivity monotonically decreases with increasing temperature, and the rate of the decrease is highest at temperatures to 600°C. The thermal diffusivity was lowest in samples based on hafnium oxide: 8, 9, 11, and 12.

From the measured specific heat, density, and thermal diffusivity, the thermal conductivity was calculated by formula (1) for 13 samples of ceramics in the system $Sm_2O_3-Y_2O_3-HfO_2$ (Fig. 6).

The most important requirements in designing TBC ceramic layers are the following:

—decrease the thermal conductivity λ;

—increase LTEC: more than $8\alpha_L$;
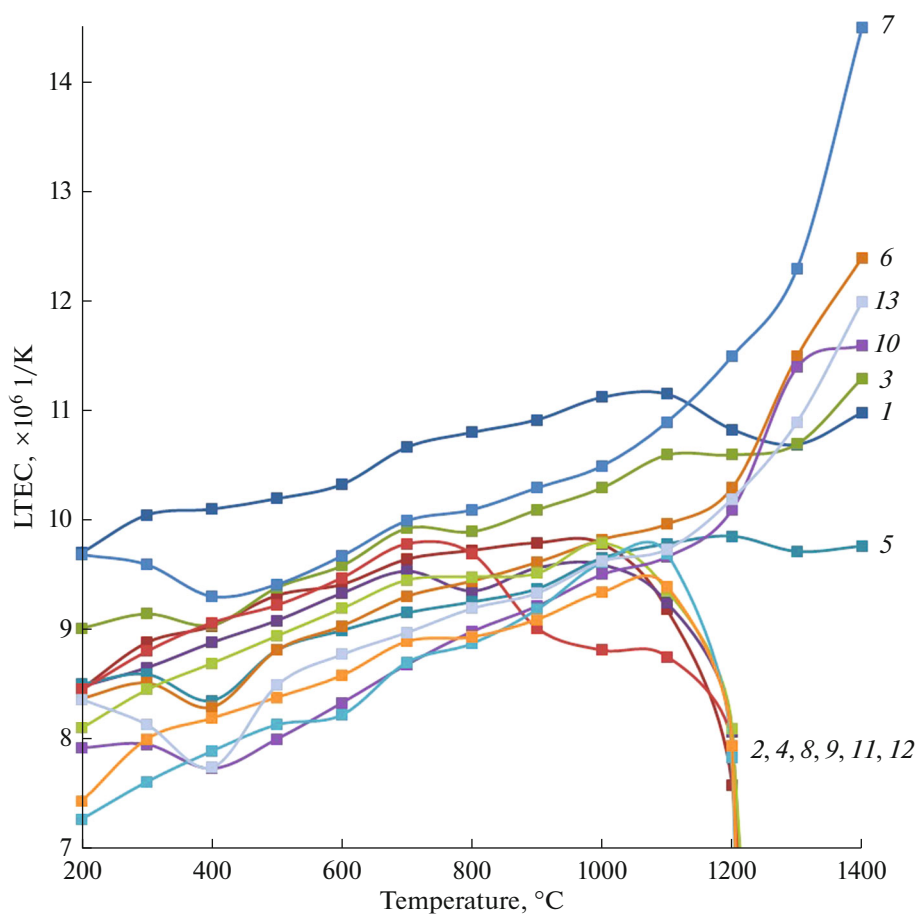
Fig. 2. Results of dilatometric measurements of LTEC of samples with the following experimental compositions: (*1*) 70% Sm_2O_3−30% Y_2O_3, (*2*) 50% Sm_2O_3−50% Y_2O_3, (*3*) 50% Sm_2O_3−50% HfO_2, (*4*) 37.5% Sm_2O_3−31.25% Y_2O_3−31.25% HfO_2, (*5*) 25% Sm_2O_3−37.5% Y_2O_3−37.5% HfO_2, (*6*) 12.5% Sm_2O_3−43.75% Y_2O_3−43.75% HfO_2, (*7*) 50% Sm_2O_3−12.5% Y_2O_3−37.5% HfO_2, (*8*) 37.5% Sm_2O_3−15.62% Y_2O_3−46.88% HfO_2, (*9*) 25% Sm_2O_3−18.75% Y_2O_3−56.25% HfO_2, (*10*) 12.5% Sm_2O_3−21.82% Y_2O_3−65.68% HfO_2, (*11*) 10% Y_2O_3−90% HfO_2, (*12*) 10% Sm_2O_3−90% HfO_2, and (*13*) 10% Sm_2O_3−10% Y_2O_3−80% HfO_2.

—decrease the LTEC deviations $\Delta\alpha_L$ (the difference of the maximal and minimal LTEC values).

For this purpose, the following characteristic function Ω of the physicochemical properties of a TBC ceramic layer was introduced:

$$\Omega = \frac{\alpha_L}{\lambda\Delta\alpha_L}. \quad (2)$$

The value of the function is the higher, the more satisfactory are the required properties of a ceramic material. To calculate Ω, the thermal conductivity λ at

Table 2. Results of calculation of the characteristic function of the physical properties of the TBC ceramic layer

Parameter	Composition												
	1	2	3	4	5	6	7	8	9	10	11	12	13
λ	1.68	0.79	0.83	0.50	1.15	1.14	1.17	0.44	0.38	0.91	0.49	0.42	0.68
$\alpha_L \times 10^6$	11.16	9.80	11.30	9.60	9.86	12.40	14.50	9.79	9.80	11.60	9.70	9.40	12.00
$\Delta\alpha_L \times 10^6$	1.45	76.0	2.28	182.6	1.50	4.10	5.19	232.8	183.8	3.86	238.7	266.4	4.25
Ω	4.59	0.16	5.99	0.11	5.69	2.66	2.38	0.10	0.14	3.31	0.08	0.08	4.17
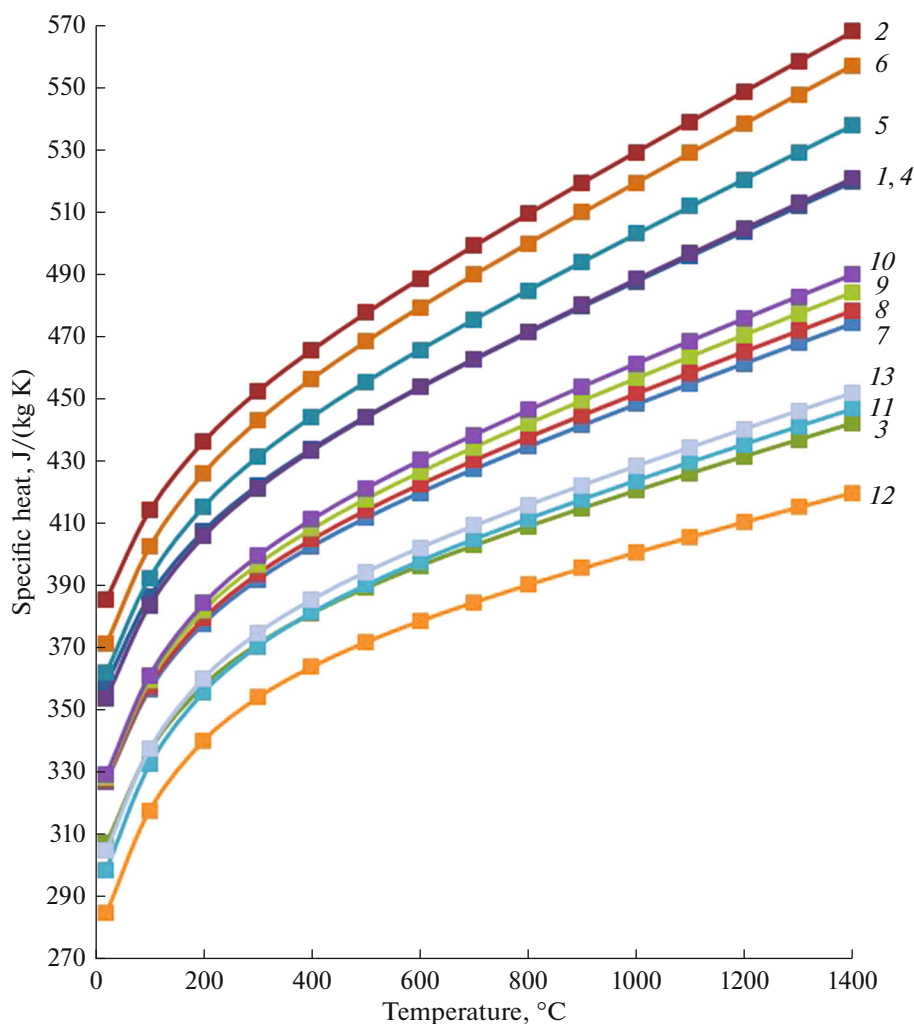
Fig. 3. Results of measurements of the specific heats of samples with the following experimental compositions (mol % as synthesized): (*1*) 70% Sm_2O_3−30% Y_2O_3, (*2*) 50% Sm_2O_3−50% Y_2O_3, (*3*) 50% Sm_2O_3−50% HfO_2, (*4*) 37.5% Sm_2O_3−31.25% Y_2O_3−31.25% HfO_2, (*5*) 25% Sm_2O_3−37.5% Y_2O_3−37.5% HfO_2, (*6*) 12.5% Sm_2O_3−43.75% Y_2O_3−43.75% HfO_2, (*7*) 50% Sm_2O_3−12.5% Y_2O_3−37.5% HfO_2, (*8*) 37.5% Sm_2O_3−15.62% Y_2O_3−46.88% HfO_2, (*9*) 25% Sm_2O_3−18.75% Y_2O_3−56.25% HfO_2, (*10*) 12.5% Sm_2O_3−21.82% Y_2O_3−65.68% HfO_2, (*11*) 10% Y_2O_3−90% HfO_2, (*12*) 10% Sm_2O_3−90% HfO_2, and (*13*) 10% Sm_2O_3−10% Y_2O_3−80% HfO_2.

1400°C, the maximum value α_L of LTEC in the range 200−1400°C, and $\Delta\alpha_L$ in the range 200−1400°C were taken. Table 2 presents the calculation results.

RESULTS AND DISCUSSION

The measurement showed that LTEC of samples 2, 4, 8, 9, 11, and 12 abruptly decreases at temperatures above 1000°C, which suggests that the crystal lattice changes at elevated experimental temperatures. The decisive effect on LTEC of sample 2 can be exerted by a polymorphic transition through a two-phase region in the Sm_2O_3−Y_2O_3 system [26, 27]. The simultaneous analysis of the results of the studies of samples 2 and 7

demonstrated that the introduction of hafnium oxide stabilizes the physicochemical properties of the Sm_2O_3−Y_2O_3 system, with the thermal conductivity changing insignificantly. The detected abrupt decrease in LTEC of sample 11 agrees well with the state diagram of the Y_2O_3−HfO_2 system [22, 23, 29] and can be explained by a transition to the monoclinic structure. The simultaneous analysis of the data on samples 11 and 13 showed that the addition of Sm_2O_3 stabilizes the Y_2O_3−HfO_2 system and is likely to prevent the transition to the monoclinic structure.

Note that, in the phase diagram of the system Sm_2O_3−Y_2O_3−HfO_2 (Fig. 1), the composition points of samples 2, 4, 9, and 12 lie on the same line, which
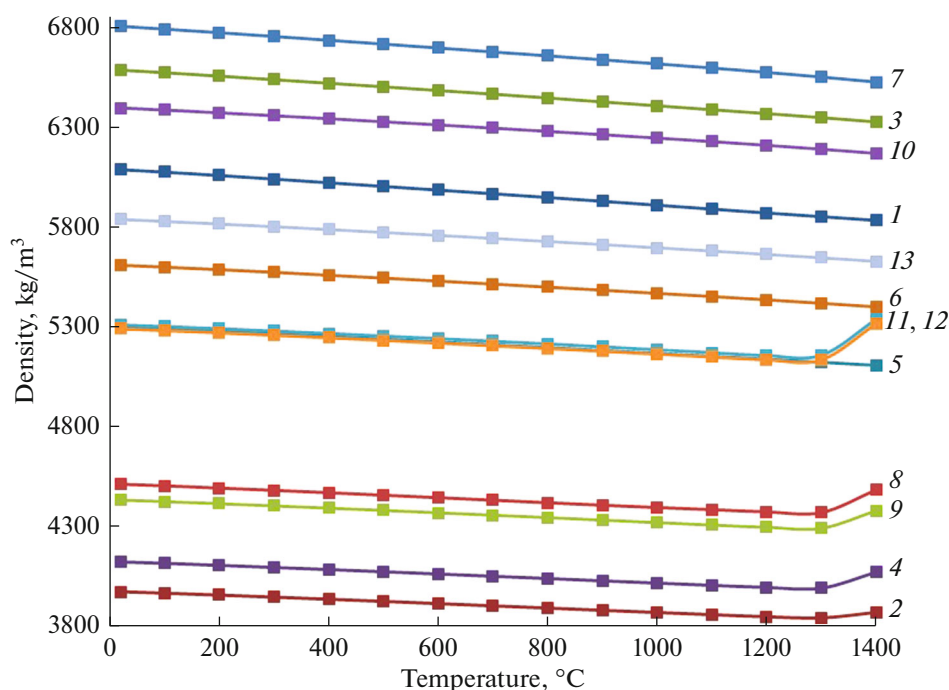
Fig. 4. Results of hydrostatic weighing measurements (A&D GR200 analytical balance) of the density of samples with the following experimental compositions (mol % as synthesized): (*1*) 70% Sm_2O_3–30% Y_2O_3, (*2*) 50% Sm_2O_3–50% Y_2O_3, (*3*) 50% Sm_2O_3–50% HfO_2, (*4*) 37.5% Sm_2O_3–31.25% Y_2O_3–31.25% HfO_2, (*5*) 25% Sm_2O_3–37.5% Y_2O_3–37.5% HfO_2, (*6*) 12.5% Sm_2O_3–43.75% Y_2O_3–43.75% HfO_2, (*7*) 50% Sm_2O_3–12.5% Y_2O_3–37.5% HfO_2, (*8*) 37.5% Sm_2O_3–15.62% Y_2O_3–46.88% HfO_2, (*9*) 25% Sm_2O_3–18.75% Y_2O_3–56.25% HfO_2, (*10*) 12.5% Sm_2O_3–21.82% Y_2O_3–65.68% HfO_2, (*11*) 10% Y_2O_3–90% HfO_2, (*12*) 10% Sm_2O_3–90% HfO_2, and (*13*) 10% Sm_2O_3–10% Y_2O_3–80% HfO_2.

is approximately described by the equation (the coefficient of determination $R^2 = 0.951$):

$$1 - \left(\frac{N_{Y_2O_3}}{N_{Sm_2O_3}}\right)^2 = N_{HfO_2}. \qquad (3)$$

Here, $N_{Y_2O_3}$, $N_{Sm_2O_3}$, and N_{HfO_2} are the mole fractions of oxides of yttrium, samarium, and hafnium, respectively. At the same time, samples 4, 8, 9, and 12 have the lowest thermal conductivities (<0.7 W/(m K)). The identical behavior of the thermal conductivity and LTEC may suggest the formation of phases of the fluorite or pyrochlore type, which are characteristic of the binary system Sm_2O_3–HfO_2. The simultaneous analysis of the change in the physicochemical properties of samples 4, 8, and 9, on the one hand, and samples 5, 6, 7, and 10, on the other, showed that insignificant variations of the contents of oxides in the system under consideration lead to changes in the phase states in the system Sm_2O_3–Y_2O_3–HfO_2 with the formation of phases similar in thermal conductivity and LTEC. Moreover, the phase stability dramatically decreases at temperatures >1000°C. The detected features of the change in the physicochemical properties should be taken into account in electron beam deposition of

coatings, when the composition of the condensate may change in comparison with the compositions of the initial components. This phenomenon may lead to a sharp change in the properties of coatings that can be obtained in the system Sm_2O_3–Y_2O_3–HfO_2.

Noteworthily, at samarium oxide content to 12.5 mol % in the system Sm_2O_3–Y_2O_3–HfO_2, LTEC remains stable in the temperature range 20–1400°C at acceptable values of the thermal conductivity of studies samples 6, 10, and 13 within the range 0.8–1.6 W/(m K). Increasing the samarium oxide content leads to variations of the phase composition and physicochemical properties, which are probably related to the interaction between Sm_2O_3 and Y_2O_3.

CONCLUSIONS

The investigation of the main thermophysical properties of samples of ceramics in the system Sm_2O_3–Y_2O_3–HfO_2 demonstrated that the introduction to 12.5 mol % samarium oxide ensures the stability of the linear thermal expansion coefficient at thermal conductivities in the range 0.8–1.6 W/(m K).

Increasing the samarium oxide content >12.5 mol % probably leads to phase instability of the system
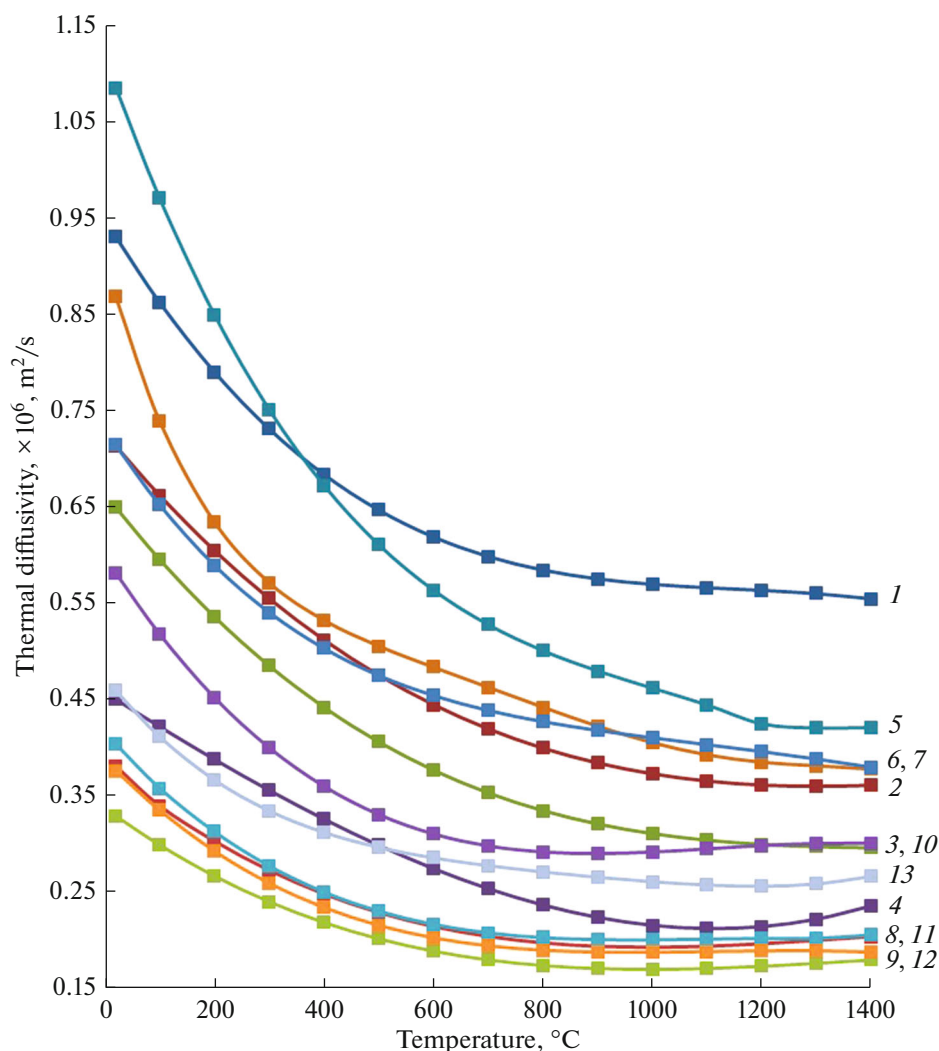
Fig. 5. Results of measurements of the thermal diffusivity of samples with the following experimental compositions (mol % as synthesized): (*1*) 70% Sm_2O_3–30% Y_2O_3, (*2*) 50% Sm_2O_3–50% Y_2O_3, (*3*) 50% Sm_2O_3–50% HfO_2, (*4*) 37.5% Sm_2O_3–31.25% Y_2O_3–31.25% HfO_2, (*5*) 25% Sm_2O_3–37.5% Y_2O_3–37.5% HfO_2, (*6*) 12.5% Sm_2O_3–43.75% Y_2O_3–43.75% HfO_2, (*7*) 50% Sm_2O_3–12.5% Y_2O_3–37.5% HfO_2, (*8*) 37.5% Sm_2O_3–15.62% Y_2O_3–46.88% HfO_2, (*9*) 25% Sm_2O_3–18.75% Y_2O_3–56.25% HfO_2, (*10*) 12.5% Sm_2O_3–21.82% Y_2O_3–65.68% HfO_2, (*11*) 10% Y_2O_3–90% HfO_2, (*12*) 10% Sm_2O_3–90% HfO_2, and (*13*) 10% Sm_2O_3–10% Y_2O_3–80% HfO_2.

Sm_2O_3–Y_2O_3–HfO_2 and to sharp variations of the linear thermal expansion coefficient at insignificant changes in the composition. This strongly complicates the use of the studied composites in electron beam deposition of coatings because of the possibility of a significant change in the composition of the condensate in comparison with the compositions of the initial components.

Among the studied samples of ceramics in the system Sm_2O_3–Y_2O_3–HfO_2, the lowest thermal conductivity (0.45–0.65 W/(m K)) was observed in the samples that demonstrated the loss of the phase stability at temperature >1000°C. The positions of their corre-

sponding composition points in the state diagram of the ternary system under investigation can be described by the equation $N_{HfO_2} = 1 - \left(\dfrac{N_{Y_2O_3}}{N_{Sm_2O_3}} \right)^2$.

The simultaneous evaluation of the variations of the linear thermal expansion coefficient and the thermal conductivity can recommend the following samples for further investigation (mol %): 10% Sm_2O_3–10% Y_2O_3–80% HfO_2, 50% Sm_2O_3–50% HfO_2, and 70% Sm_2O_3–30% Y_2O_3, and also 25% Sm_2O_3–37.5% Y_2O_3–37.5% HfO_2.
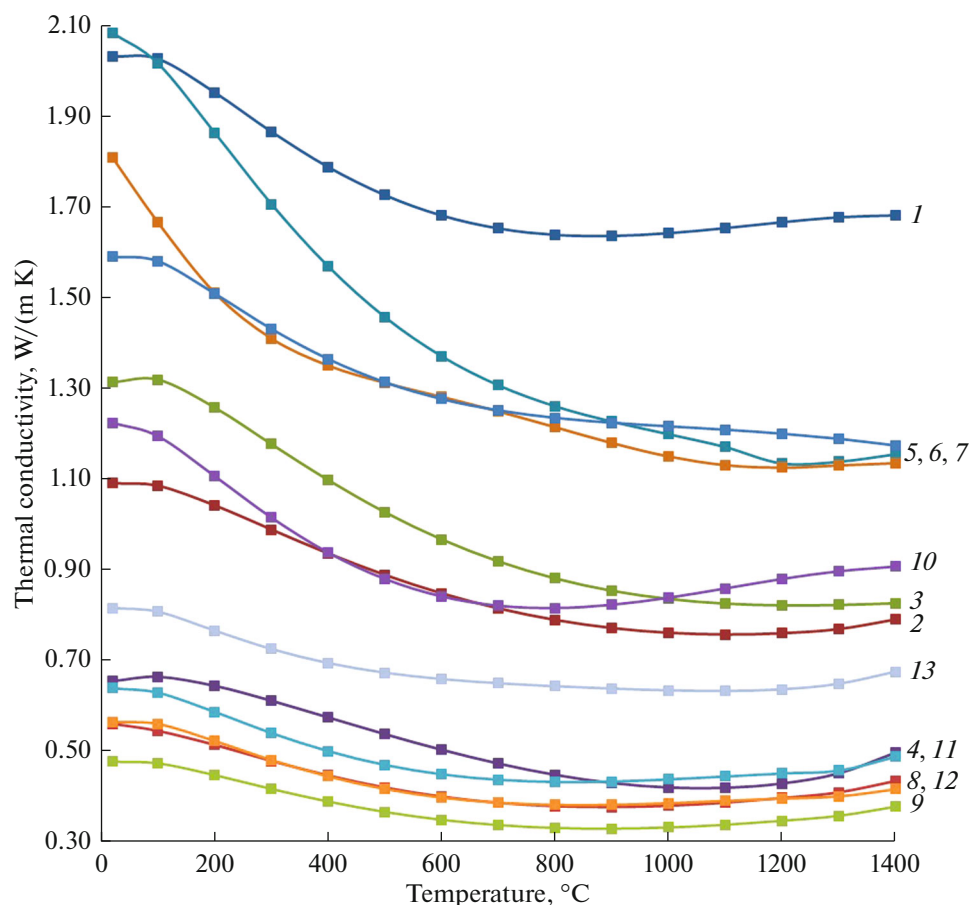
Fig. 6. Calculated thermal conductivity of samples with the following experimental compositions (mol % as synthesized): (*1*) 70% Sm_2O_3−30% Y_2O_3, (*2*) 50% Sm_2O_3−50% Y_2O_3, (*3*) 50% Sm_2O_3−50% HfO_2, (*4*) 37.5% Sm_2O_3−31.25% Y_2O_3−31.25% HfO_2, (*5*) 25% Sm_2O_3−37.5% Y_2O_3−37.5% HfO_2, (*6*) 12.5% Sm_2O_3−43.75% Y_2O_3−43.75% HfO_2, (*7*) 50% Sm_2O_3−12.5% Y_2O_3−37.5% HfO_2, (*8*) 37.5% Sm_2O_3−15.62% Y_2O_3−46.88% HfO_2, (*9*) 25% Sm_2O_3−18.75% Y_2O_3−56.25% HfO_2, (*10*) 12.5% Sm_2O_3−21.82% Y_2O_3−65.68% HfO_2, (*11*) 10% Y_2O_3−90% HfO_2, (*12*) 10% Sm_2O_3−90% HfO_2, and (*13*) 10% Sm_2O_3−10% Y_2O_3−80% HfO_2.

CONFLICT OF INTEREST

The authors declare that they have no conflicts of interest.

REFERENCES

1. E. N. Kablov, Aviats. Mater. Tekhnol., No. 1, 3 (2015). https://doi.org/10.18577/2071-9140-2015-0-1-3-33

2. D. S. Kashin and P. A. Stekhov, Tr. Vses. Nauchno-Issled. Inst. Aviats. Mater., No. 2, 10 (2018). https://doi.org/10.18577/2307-6046-2018-0-2-10-10

3. D. E. Kablov, V. V. Sidorov, S. A. Budinovskii, and P. G. Min, Aviats. Mater. Tekhnol., No. 1, 20 (2016). https://doi.org/10.18577/2071-9140-2016-0-1-20-23

4. E. N. Kablov, O. G. Ospennikova, and I. L. Svetlov, Aviats. Mater. Tekhnol., No. 2, 3 (2017). https://doi.org/10.18577/2071-9140-2017-0-2-3-14

5. E. N. Kablov, O. G. Ospennikova, and N. V. Petrushin, Aviats. Mater. Tekhnol., No. 1, 34 (2015). https://doi.org/10.18577/2071-9140-2015-0-1-34-40

6. E. N. Kablov, O. G. Ospennikova, N. V. Petrushin, et al., Aviats. Mater. Tekhnol., No. 2, 14 (2015). https://doi.org/10.18577/2071-9140-2015-0-2-14-25

7. K. W. Schlichting, N. P. Padture, and P. G. Klemens, J. Mater. Sci., **36**, 3003 (2001). https://doi.org/10.1023/A:1017970924312

8. D. A. Chubarov and P. V. Matveev, Aviats. Mater. Tekhnol., No. 4, 43 (2013).

9. S. A. Budinovskii, A. A. Smirnov, P. V. Matveev, et al., Tr. Vses. Nauchno-Issled. Inst. Aviats. Mater., No. 4, 105 (2015). https://doi.org/10.18577/2307-6046-2015-0-4-5-5

10. G. V. Samsonov, A. L. Borisova, et al., *Physicochemical Properties of Oxides: A Reference Book* (Metallurgiya, Moscow, 1978) [in Russian].

11. Kazuhide Matsumoto, Yoshiyasu Itoh, and Tsuneju Kameda, Sci. Technol. Adv. Mater., **4**, 153 (2003). https://doi.org/10.1016/S1468-6996(03)00009-3

12. N. I. Grechanyuk, P. P. Kucherenko, I. N. Grecha-nyuk, et al., Mizhvuz. Zb. Nauk. Notatki, No. **31**, 92 (2011).

13. I. Gurrappa and A. Sambasiva Rao, Surf. Coat. Technol. **201**, 3016 (2006).
https://doi.org/10.1016/j.surfcoat.2006.06.026

14. Chong Wang, M. Zinkevich, and F. Aldinger, Pure Appl. Chem. **79**, 1731 (2007).
https://doi.org/10.1351/pac200779101731

15. C. V. Ramana and R. A. Choudhuri, UTSR Workshop, 2012.
https://doi.org/10.2172/1132566

16. Y. I. Folomeikin, F. N. Karachevtsev, and V. L. Stol-yarova, Russ. J. Inorg. Chem. **64**, 934 (2019).
https://doi.org/10.1134/S0036023619070088

17. G. Moscal and L. Swadzba, et al., J. Eur. Ceram. Soc. **32**, 2025 (2012).
https://doi.org/10.1016/j.jeurceramsoc.2011.11.043

18. Hengbei Zhao, M. R. Begley, A. Heuer, et al., Surf. Coat. Technol. **205**, 4355 (2011).
https://doi.org/10.1016/j.jeurceramsoc.2011.03.028

19. V. N. Guskov, K. S. Gavrichev, P. G. Gagarin, et al., Russ. J. Inorg. Chem. **64**, 1265 (2019).
https://doi.org/10.1134/S0036023619100048

20. E. V. Didnik and S. N. Lakiza, et al., Powder Metall. Met. Ceram. **57**, 301 (2018).
https://doi.org/10.1007/s11106-018-9983-z

21. Thermal Spray Materials Guide. www.oerlikon.com/ecomaXL/files/metco/oerlikon_BRO-0001.17_TS_MaterialGuide_EN.pdf (accessed October 31, 2019).

22. B. Sundman, B. Jansson, and J. O. Andersson, CALPHAD: Comput. Coupling Phase Diagrams Thermochem. **9**, 153 (1985).

23. A. V. Shevchenko, L. M. Lopato, and I. E. Kir'yakova, Izv. Akad. Nauk SSSR, Neorg. Mater. **20**, 1991 (1984).

24. E. R. Andrievskaya and L. M. Lopato, in *Proc. Int. Conf. on Solid-to-Solid Phase Transformations in Inorganic Materials (PTM'94), Farmington, PA, July 17–22, 1994*, Ed. by W. C. Johnson (Miner. Met. Mater. Soc., Pittsburg, PA, 1994), p. 125.

25. O. R. Andrievskaya, Doctoral Dissertation in Chemistry (Kiev, 2003).

26. L. M. Lopato, B. S. Nigmanov, A. V. Shevchenko, et al., Izv. Akad. Nauk SSSR, Neorg. Mater. **22**, 771 (1986).

27. M. Foex and J. P. Traverse, Rev. Int. Hautes Temp. Refract. **3**, 429 (1966).

28. E. N. Kablov, V. L. Stolyarova, V. A. Vorozhtcov, et al., Rapid Commun. Mass Spectrom. **34**, e8693 (2019).
https://doi.org/10.1002/rcm.8693

29. A. V. Shevchenko, L. M. Lopato, and Z. A. Zaitseva, Izv. Akad. Nauk SSSR, Neorg. Mater. **20**, 1530 (1984).

30. M. A. Mikheev and I. M. Mikheeva, *Physical Foundations of Heat Transfer* (Energiya, Moscow, 1977) [in Russian].

Translated by V. Glyanchenko